Advances in Geo-Energy Research

Vol. 18, No. 2, p. 99-108, 2025

Original article

Wetting and injecting effects on CO_2 distribution: Pore-scale micromodel and simulation

Jiaxin Shao[1,2,3], Zimeng Wang[1,2], Binglin Huang[1,2], Xiangyun Shi[4], Ziqing Pan[1,2], David Misch[4], Kaiqiang Zhang[1,2,5]*

[1]*Institute of Energy, Peking University, Beijing 100871, P. R. China*

[2]*Ordos Research Institute of Energy, Peking University, Ordos 017010, P. R. China*

[3]*State Key Laboratory of Oil and Gas Reservoir Geology and Exploitation, Southwest Petroleum University, Chengdu 610500, P. R. China*

[4]*Department of Applied Geosciences and Geophysics, Technical University of Leoben, Leoben 8700, Austria*

[5]*Institute of Carbon Neutrality, Peking University, Beijing 100871, P. R. China*

Keywords:
CO_2 storage
wettability
CO_2 distribution
micromodel

Cited as:
Shao, J., Wang, Z., Huang, B., Shi, X., Pan, Z., Misch, D., Zhang, K. Wetting and injecting effects on CO_2 distribution: Pore-scale micromodel and simulation. Advances in Geo-Energy Research, 2025, 18(2): 99-108.
https://doi.org/10.46690/ager.2025.11.01

Abstract:
The distribution of CO_2 is critical to the efficiency and stability of carbon storage; however, the roles of wettability and capillary number in controlling CO_2 distribution remain inadequately understood. In this study, visual waterflooding experiments and numerical simulations were performed using five homogeneous micromodels with distinct wettability characteristics to examine how wettability and capillary number influence CO_2 distribution during short-term waterflooding. The results demonstrate that both wettability and capillary number govern CO_2 distribution patterns and saturation. These patterns include continuous distribution, cluster-like distribution, and isolated bubbles. Both experimental and simulation data reveal that the total residual CO_2 saturation follows a non-monotonic trend with increasing contact angle, while it increases as the capillary number decreases. As the capillary number varies, the displacement behavior transitions gradually from a stable displacement regime to a capillary fingering regime, resulting in variations in residual CO_2 saturation. With changing wettability, cooperative pore filling leads to fluid bypassing, thereby modifying the saturation of continuously distributed CO_2. In contrast, variations in the saturation of cluster-like and isolated bubble CO_2 are attributed to snap-off mechanisms initiated by preceding film flow. This study elucidates how wettability and capillary number govern the residual trapping and distribution of CO_2 at the pore scale.

1. Introduction

Multiphase displacement in porous media is a ubiquitous phenomenon in both natural and industrial settings, such as geological CO_2 storage, enhanced oil and gas recovery, plant water uptake, and drug delivery in the bloodstream (Ayush and Francesco, 2010; Tannaz et al., 2020; Mohsen et al., 2022; Zou et al., 2024). Wettability variations are a primary factor influencing multiphase displacement behavior in porous media. Moreover, the wettability conditions significantly influence the distribution of fluids during the process of non-miscible multiphase fluid displacement within porous media (Hu et al., 2017; Cai et al., 2024a). In CO_2 sequestration and enhanced oil recovery, for instance, the miscibility of CO_2 with crude oil leads to a substantial reduction in interfacial tension, enabling the simultaneous achievement of CO_2 storage and improved oil recovery (Salathiel, 1973; Zhang et al., 2018; Li et al., 2021, 2024). During water injection for enhanced oil recovery, the addition of surfactants to the displacing fluid

Yandy Scientific Press

*Corresponding author.
E-mail address: 18582497091@163.com (J. Shao); 2501110668@stu.pku.edu.cn (Z. Wang); 2501110679@stu.pku.edu.cn (B. Huang); xiangyun.shi@unileoben.ac.at (X. Shi); ziqing.pan@pku.edu.cn (Z. Pan); David.Misch@unileoben.ac.at (D. Misch).

Received August 12, 2025; revised September 7, 2025; accepted September 25, 2025; available online September 29, 2025.

modifies the wettability between the fluid and the reservoir rock, leading to an increase in the area contacted by the injected fluid (Magali and Yukie, 2017; Zhang et al., 2019).

Geological CO_2 storage offers a significant strategy for reducing carbon emissions from major industrial sources, including power generation from fossil fuels and cement manufacturing, thus contributing to the climate change mitigation (Drange et al., 2001; Sabine and Tanhua, 2010; Li et al., 2022b; Wang et al., 2023b). The injection of CO_2 into porous subsurface rock formations leads to the displacement of existing pore fluids, including brine and oil. Following the cessation of injection, a flowback of these fluids may occur, resulting in the partial displacement of the injected CO_2 (Suekane et al., 2009; Perrin and Benson, 2010). The complex displacement behavior of these immiscible fluids within the porous rock matrix leads to the trapping of some CO_2 within pore spaces, a process known as residual or capillary trapping (Shi et al., 2011).

Capillary forces and viscous forces have a significant impact on the capillary trapping of CO_2. The competition between viscous and capillary forces is characterized by the classical macroscopic capillary number, Ca (Zhang et al., 2011; Chaudhary et al., 2013; Geistlinger et al., 2015). The classic macroscopic capillary number fails to consider the fundamentally different scales on which viscous and capillary forces act. Specifically, it does not distinguish between the nonlocal, volumetric nature of viscous forces and the local action of capillary forces at the menisci interfaces (Blunt and Scher, 1995; Armstrong et al., 2014).

The displacement pattern and flow regime of immiscible fluids in porous media are influenced by the capillary number, Ca ($\mathrm{Ca} = \mu v/\sigma$), and the viscosity ratio, M ($M = \mu_1/\mu_2$), where v is the velocity of the invading fluid, σ is the interfacial tension between the invading and defending fluids, and μ_1 and μ_2 are the viscosities of the invading fluid (e.g., CO_2) and the defending fluid (e.g., water), respectively (Zhang et al., 2011; Chaudhary et al., 2013; Geistlinger et al., 2015). Wettability also influences the capillary trapping and distribution of CO_2. Oil-wet or CO_2-wet media trap less CO_2 compared to water-wet media (Iglauer et al., 2012; Rahman et al., 2016). However, Plug and Bruining (2007); Tokunaga and Wan (2013); Wang et al., 2016) suggest that more non-wetting phase becomes trapped as the wettability of the porous medium decreases. A smaller contact angle of the invading fluid may be a key mechanism leading to increased CO_2 trapping. On the other hand, under strongly water-wet conditions, the dominant process is considered to be cooperative pore filling. During imbibition, pore-scale multiphase flow behavior involves additional complexities, such as the influence of pore surface roughness, the impact of contact angle hysteresis, and the heterogeneity of the porous medium. Although the influence of wettability on CO_2 trapping has been extensively studied, there is limited research and evidence in the literature regarding the non-monotonic behavior of CO_2 capillary trapping, as well as its distribution patterns.

Two-dimensional (2D) micromodel experiments provide an effective means of investigating pore-scale multiphase flow, allowing for direct observation of real-time fluid movement (Cai et al., 2024b; Wang et al., 2023a). Lei et al. (2024) systematically investigated the influence of micromodel width-to-depth ratio on interfacial instability during wetting fluid displacement of a non-wetting fluid in porous media, using micromodel experiments. Lei et al. (2023) investigated the effect of wettability on multiphase displacement in disordered porous media under preferential flow conditions using a heterogeneous micromodel. Chang et al. (2020) conducted experiments using a 2.5D mixed-wettability micromodel to investigate the displacement of brine by supercritical CO_2 at 8.5 MPa and 45 °C, analyzing the impact of unstable displacement on CO_2 storage efficiency. By combining theoretical derivation, numerical simulations and micromodel experiments, Li et al. (2022a) modeled and verified the spontaneous imbibition phenomenon under the effect of gravity in porous medium. For similar purpose, micromodel experiments regarding Carbonated water injection has been design and conducted by Chen et al. (2025). Their focus is mainly on capillary number and viscosity ratio relation. They found that in such systems, liquid-vapor interfaces near the vaporization front dominated phase changes, while interfaces away from vaporization front contributed minimally. Yuan et al. (2023) studied capillary imbibition by conducting experiments on heterogeneous matrix-fracture micromodels.

They concluded that the imbibition pattern is dictated by the boundary condition and remains independent of the applied driving pressure.

Previous studies have mostly focused on the process of CO_2 injection into formations, with less attention given to the effects of wettability and injection effects on CO_2 distribution during water reflux. This study employs microfluidic experiments and numerical simulation methods to simulate water reflux behavior during CO_2 storage and systematically classify the distribution patterns of CO_2. The changes in CO_2 saturation after displacement breakthrough were qualitatively and quantitatively characterized. Finally, based on image processing methods, the saturation of CO_2 under different distribution patterns was quantitatively characterized, revealing the mechanisms of capillary number and wettability on CO_2 distribution.

2. Materials and methods

2.1 Numerical simulation

This study employs numerical simulation software to achieve pore-scale simulation of water displacing CO_2 through key procedures including microscopic visualization model construction, mesh generation, parameter configuration, and result processing. First, create the model required for the simulation, ensuring that the created geometric model is consistent with the dimensions of the micromodel. After the geometric model is created, select and name the inlets, outlets, boundaries, and cylinders of the model, then proceed to mesh generation based on the simulation conditions (Fig. 1). Then, set the boundary conditions, inlet conditions, and outlet conditions for the numerical simulation according to the microfluidic experimental conditions.

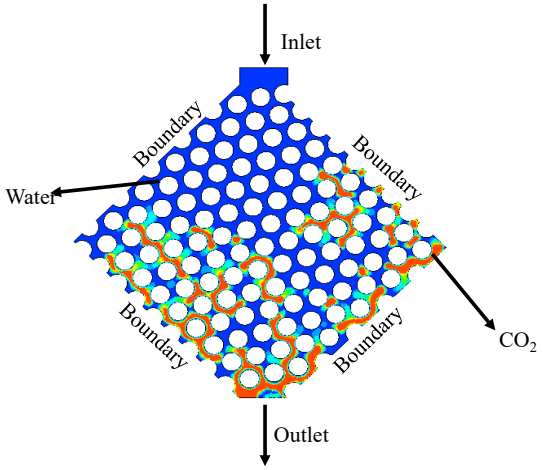

Fig. 1. Schematic diagram of the micromodel for numerical simulation.

For pore-scale porous medium flow, fluid follows the continuity equation and Navier-Stokes (Peter, 1990):

$$\nabla \cdot \vec{v} = 0$$
$$\rho\left(\frac{\partial \vec{v}}{\partial t} + \vec{v} \cdot \nabla \cdot \vec{v}\right) = -\nabla P + \mu \Delta \vec{v} \quad (1)$$

where $\vec{v}$ is the velocity of the fluid, ρ is the density of fluid, P is the pressure of the fluid, μ is the fluid viscosity, t is the time. Gravity term is neglected in this simulation since its 2D nature. For boundary conditions, the inlet is set as mass flow rate boundary condition, where the mass flow rate is 0.1-0.001 mL/min. The outlet boundary condition is set as outflow condition. As for boundary conditions at walls, non-slip condition is adopted. As for initial conditions, at the beginning of the simulations, velocity on all needs are set as 0, and the percentage of CO_2 is set as 0 (or 1). Since this paper is about CO_2-water injection, a two phase model, volume of fluid method is adopted for the CO_2-water interface interactions. A 2D mesh with 40,000 nodes is applied.

2.2 Experimental section

2.2.1 Visual equipment

The micromodel visualization system comprises a CO_2 cylinder, a high-pressure displacement pump (ISCO SyriXus 260X), a 200 ml intermediate vessel for the displacing fluid (Deionized water), a micromodel, and an imaging system (Fig. 2). The CO_2 cylinder provides the gas source, and a flow meter controls the filling of the micromodel. A high-pressure displacement pump provides the driving force to inject water (Invading fluid) from the intermediate vessel, displacing the pre-existing CO_2 (Defending fluid) within the micromodel. The entire experimental system was housed in a sealed environment maintained at a controlled temperature.

The imaging system comprises a compound microscope (Leica 216 APO), a camera (C3 Camera), and a light source (AD-HFL7070-W) to record the pore-scale network within the micromodel. The apochromatic zoom system (16 : 1 zoom ratio, 0.57-9.2x magnification) featured a central beam path, a 1.0x Planapo Z objective lens (97 mm working distance, 29.5 mm maximum field of view), and a 1 μm resolution. The C3 camera is a digital color camera with a 1/2.3" CMOS sensor, capable of standalone operation and providing a 4K 60 fps live image output.

2.2.2 Micromodel

The micromodel was fabricated by etching borosilicate glass from SCHOTT AG (Germany). The micromodel has a pressure rating of 2 MPa and a temperature rating of approximately 500 °C. The micromodel was fabricated using wet etching with hydrofluoric acid (HF), creating a pore structure with a defined aspect ratio and pattern according to the designed physical model (Fig. 3). Two float glass substrates were used in the etching process; one served as the etching substrate, and the other as the cover plate. After etching the microchannels into the substrate and drilling access holes in the cover plate, the two glass pieces were anodically bonded to create a complete experimental micromodel. 1H, 1H, 2H, 2H-Perfluorodecyl triethoxysilane (FAS-17) was used as the wetting agent for the micromodel modification. The fluorosilane and anhydrous ethanol (1:50 mass ratio) were mixed in a clean, dry beaker and vigorously stirred using a magnetic stirrer for 1-1.5 h at room temperature. The micromodel samples were then immersed in the fluorosilane-ethanol solution for 2 h at 60 °C. After removal, the samples were dried in an oven at 120 °C for 1 h to modify the micromodel's wettability. Using the method described above, three micromodels with different wettability were prepared: Strongly water-wet (21°), moderately water-wet (33°), weakly water-wet (62°), neutral condition (82°), and hydrophobic (101°).

2.2.3 Experimental procedures

The prepared micromodel was placed on the microscope stage. The ISCO pump was then activated in suction mode to draw liquid into the pump, with distilled water supplied from an intermediate vessel. The ISCO pump was then operated in discharge mode to introduce distilled water into the micromodel, which facilitated the removal of air. Subsequently, the CO_2 cylinder was opened, and the pressure was controlled via a flow meter. The CO_2 was injected into the micromodel at a low pressure to displace the distilled water. This injection continued for an additional 0.5 h after the micromodel became saturated with CO_2 to ensure complete filling. Finally, the ISCO pump was switched to discharge mode to displace distilled water from the intermediate vessel into the micromodel at flow rates of 0.1, 0.01, and 0.001 mL/min, simulating CO_2 capillary trapping. Displacement experiments of CO_2 by distilled water were conducted in micromodels with different wettability (Table 1).

2.2.4 Image analysis

To avoid affecting the micromodel pore surface wettability, no staining agents were used. Prior to the experiments, the total pore area of the micromodel was determined using Image J software (Fig. 4(a)). Following the water-CO_2 displacement experiment, the distribution of the invading (water) and defending (CO_2) fluids was further analyzed, focusing on CO_2 distribution; therefore, different colors were used to distinguish

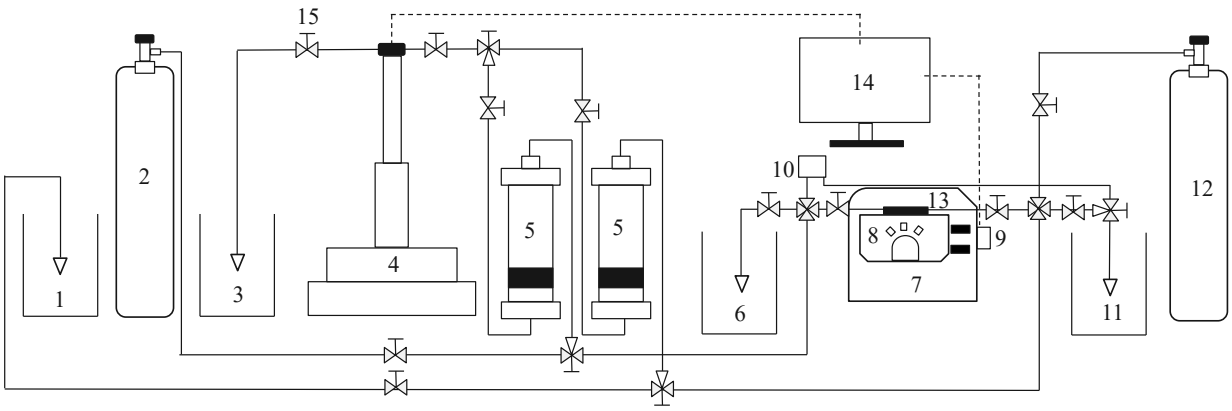

Fig. 2. Schematic diagram of the micromodel visualization experimental setup. Flow system: 1-Experimental fluid, 2-CO_2 cylinder, 3-Deionized water, 12-CO_2 cylinder, 15-Valve; Displacement system: 4-ISCO pump, 5-Intermediate vessel; Measuring system: 6-Waste fluid, 7-Heating unit, 8-Microscope, 9-Camera, 10-Pressure sensor, 11-Waste fluid, 13-Micromodel, 14-Computer.

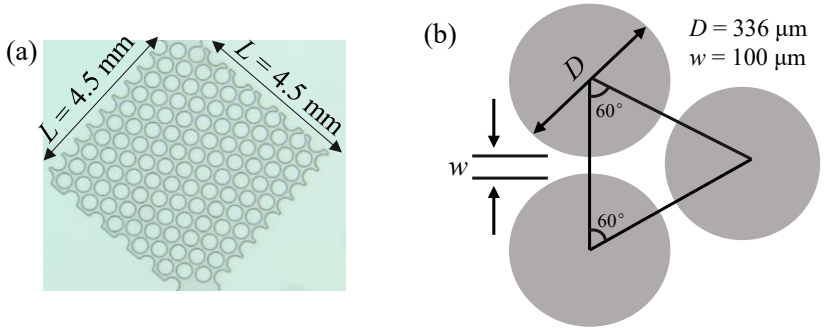

Fig. 3. Micromodel visualization: (a) Microscopic image of the micromodel, composed of 103 circular silica particles and (b) micromodel pattern (depth $d = 45$ μm); Pore throat width = 100 μm.

between different distribution patterns. Image processing was conducted to segment the water and gas phases at initial state and steady state after water flooding. Under the observation light, the water and CO_2 phases show distinct contrast. Water is light color similar to the background color, while the gas phase appears grey (Fig. 4(b)). Manual corrections were applied in case of nonuniform light intensity across the image. A binary image of the gas phase was obtained through thresholding, and the gas-filled area was quantified as a percentage of the total image area using the "Particle Analysis" function in ImageJ. For steady-state images after water invasion, segmentation was performed using the machine learning-based Pixel Classification workflow in ilastik. Due to the similarity in color between the water phase and the background, four classes were defined in the workflow: Background, residual gas phase, boundaries of gas-filled regions, and boundaries of water-saturated regions. This process involved manual annotation of each class and iterative model predictions until satisfactory segmentation was achieved. Due to the strong contrast of gas phase against the background, the gas phase in initial state images can be easily segmented using the auto thresholding method in ImageJ. The CO_2 distribution was divided into three patterns, represented by different colors: Continuous distribution (green), clustered distribution (blue), and isolated CO_2 bubble distribution (red) (Fig. 4(c)). The areas of these residual gas regions were calculated as percentages of the total image area using the "Particle Analysis" function in ImageJ.

3. Results and discussion

3.1 CO_2 capillary trapping

The numerical simulations reveal that CO_2 spatial organization after water breakthrough manifests three characteristic regimes percolating continuous pathways, disconnected ganglion clusters, and individual trapped bubbles, consistent with the experimentally observed morphological patterns (Fig. 5). The morphology of continuous distribution differs between simulation and experiment, with numerical results showing fewer large-scale continuous clusters but rather more filamentary structures traversing multiple pores. Under all wettability conditions examined, the residual trapping saturation of CO_2 consistently decreases with increasing capillary number (Fig. 5). During our initial stage of the study, numerical simulation has been applied to investigate CO_2 residual trapping and distribution during water backflow. However, it was found that while numerical simulation can reflect the total CO_2 residual trapping saturation, it has limitations in characterizing the distribution of CO_2. Also, there are other issues like phase mixing. Therefore, microscopic visualization experiments were conducted to complement the study, which clarified the distri-

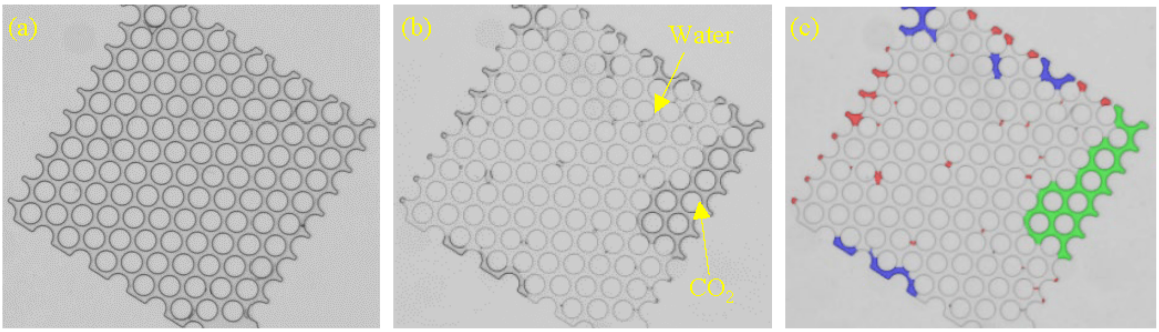

Fig. 4. Micromodel fluid distribution processing: (a) The total pore area in the CO_2-saturated state, (b) the residual CO_2 area after water displacement and (c) the CO_2 area by different distribution patterns after water displacement.

Table 1. Summary of experiment conditions.

No.	Wettability	Q (mL/min)	Ca
1	Strongly water-wet	0.1	1.0×10^{-3}
		0.01	1.0×10^{-4}
		0.001	1.0×10^{-5}
2	Moderately water-wet	0.1	1.0×10^{-3}
		0.01	1.0×10^{4}
		0.001	1.0×10^{-5}
3	Weakly water-wet	0.1	1.0×10^{-3}
		0.01	1.0×10^{-4}
		0.001	1.0×10^{-5}
4	Neutral condition	0.1	1.0×10^{-3}
		0.01	1.0×10^{4}
		0.001	1.0×10^{-5}
5	Hydrophobic	0.1	1.0×10^{-3}
		0.01	1.0×10^{-4}
		0.001	1.0×10^{-5}

bution patterns of CO_2.

The experiments employed water injection at 0.1, 0.01, and 0.001 mL/min, resulting in a range of capillary numbers from 1×10^{-3} to 1×10^{-5}. Under all experimental conditions, the CO_2 saturation reached a relatively stable state approximately 10-20 s after water breakthrough at the bottom of the micromodel. The focus of this study is to investigate the distribution patterns of CO_2 during residual trapping at the pore scale over a short period. The image captured immediately after water breakthrough at the bottom of the micromodel was selected as a representative of the water invasion process. The CO_2 distribution patterns include large continuous patches, clustered patterns spanning and connecting multiple pores, and isolated bubbles in contact with pore walls. Under the same wettability conditions, the higher the displacement flow rate of the fluid, the lower the residual CO_2 saturation (Fig. 6). This is because, at higher flow rates, the greater viscous pressure drop causes CO_2 to mobilize and be removed from the micromodel. The displacement results show that the CO_2 saturation in the moderately hydrophilic model is higher than that in the strongly and weakly hydrophilic models, while the CO_2 saturation in the intermediate-wet model is close to that in the moderately hydrophilic model. This trend remains consistent across all displacement flow rates. At the highest displacement flow rate, a considerable difference in CO_2 saturation is observed between the weakly hydrophilic and moderately hydrophilic models. If the capillary number is further reduced to approach typical reservoir flow conditions, this discrepancy would become even more pronounced. However, as the capillary number increases, the influence of wettability on CO_2 saturation diminishes progressively. If the capillary number is further increased to the extent that capillary forces become negligible and viscous forces dominate, the wettability effect is expected to diminish.

3.2 CO_2 distribution

3.2.1 Quantitative distribution patterns

To further quantitatively describe the CO_2 distribution patterns and its saturation, we used ImageJ to colorize Fig. 6. The CO_2 distribution was categorized into three patterns, denoted by different colors: Continuous distribution (green), clustered distribution (blue), and isolated CO_2 bubble distribution (red) (Fig. 7). After displacement, compared to the weakly water-wet and hydrophobic models, the CO_2 in the water-wet model is predominantly distributed at the edges of the model, with less distribution in the center. Under any wettability condition, as the capillary number decreases, the overall total saturation of residual CO_2 (defending fluid) tends to increase, while the water saturation (invading fluid) tends to decrease. This indicates that lower capillary number are more favorable for CO_2 capillary trapping. The total number of isolated CO_2 bubbles in both the water-wet and hydrophobic models was greater than that in the weakly water-wet model (Fig. 7). This is because continuous and clustered CO_2 broke down, producing isolated CO_2 bubbles. In the weakly water-wet model, the displacement process is much more dominant than the breakup of continuous and clustered CO_2, leading to a reduction in the number of isolated CO_2 bubbles. Evidence of breakup events exists from core flooding in carbonate rocks (Pak et al., 2015) and

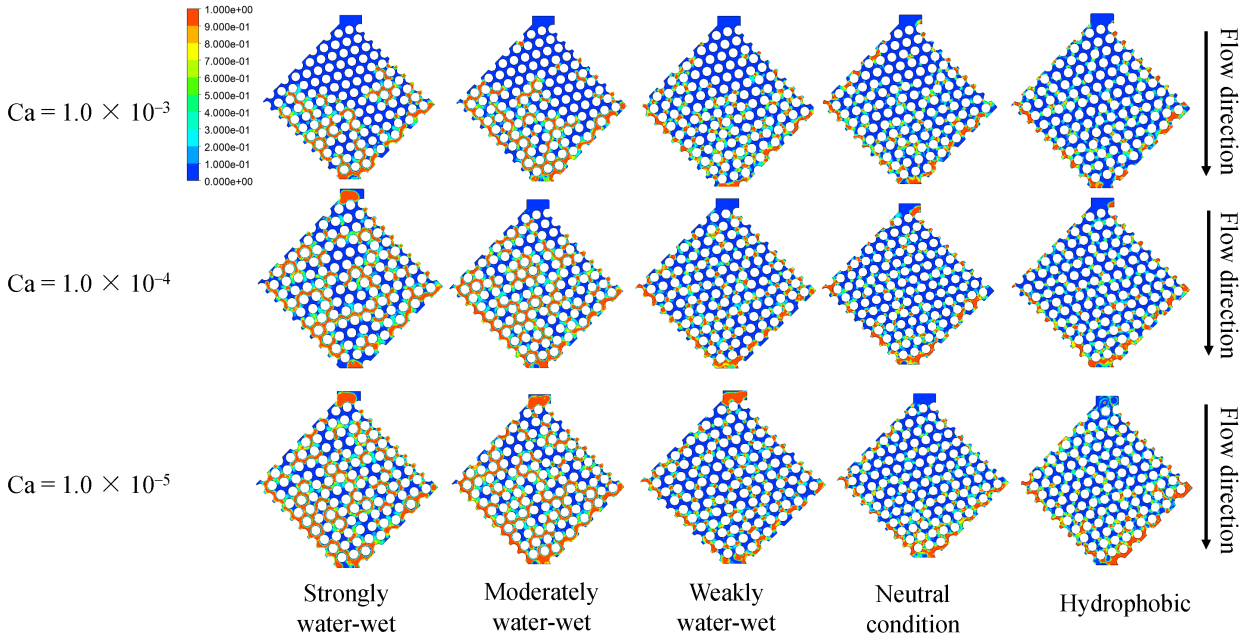

Fig. 5. Numerical simulation contour results of water flooding CO_2 under different displacement flow rates after breakthrough. The yellow regions represent the residual CO_2, while the blue regions correspond to the aqueous phase.

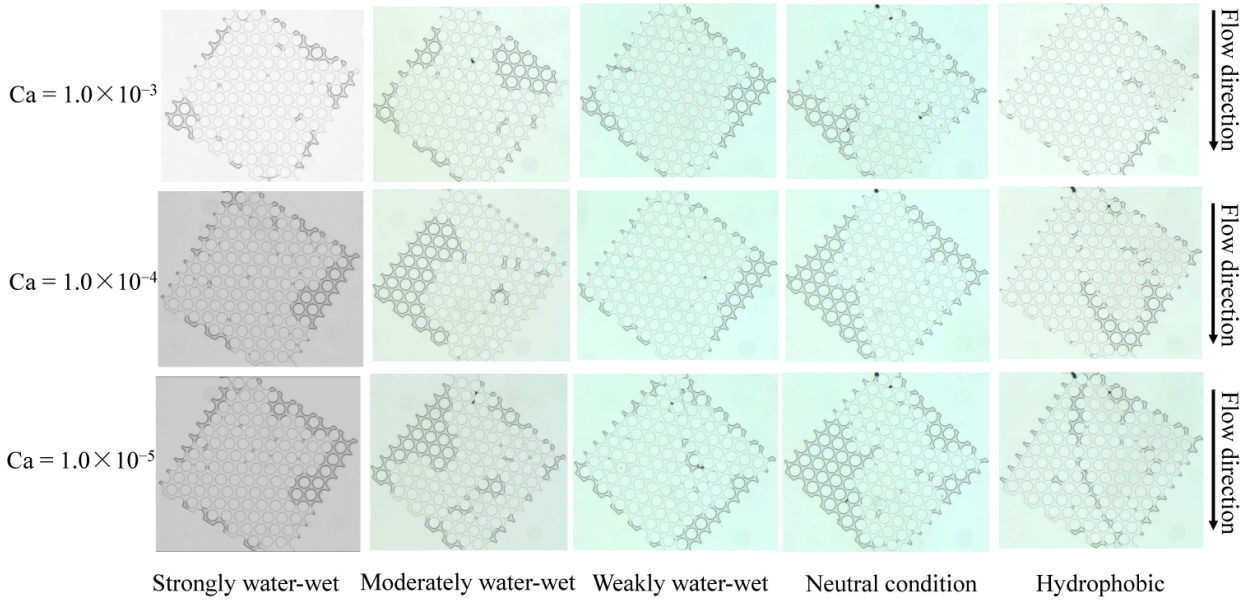

Fig. 6. Experimental results of water flooding CO_2 under different injection flow rates after breakthrough. The dark areas indicate residual CO_2, while water and solid phases are shown in light colors.

glass bead packs (Wardlaw and McKellar, 1985) to stochastic simulations (Ng and Payatakes, 1980). The isolated bubbles and the disconnected invasion fluid pathways inhibited water invasion through the Jamin effect. The Jamin effect refers to the flow resistance generated by fluid deformation during two-phase flow within pore throats, a phenomenon resulting from the difference in capillary pressures across a trapped fluid.

3.2.2 Distribution of CO_2 saturation

Under different wettability conditions, the total residual CO_2 saturation (from experiments and numerical simulations), the experimentally obtained saturation of continuously distributed CO_2, and the experimentally obtained sum of cluster-like and isolated CO_2 saturations were calculated and analyzed (Figs. 8(a)-8(d)). At the same capillary number, the total capillary trapping of CO_2 saturation exhibits a non-monotonic trend with increasing contact angle. Under the same wettability conditions, the total capillary trapping of CO_2 saturation tends to increase with decreasing capillary number (Fig. 8(a)). While differences are observed between the numerical simulation and experimental results during the transition from weakly water-wet to neutral condition, the total capillary trapping of CO_2

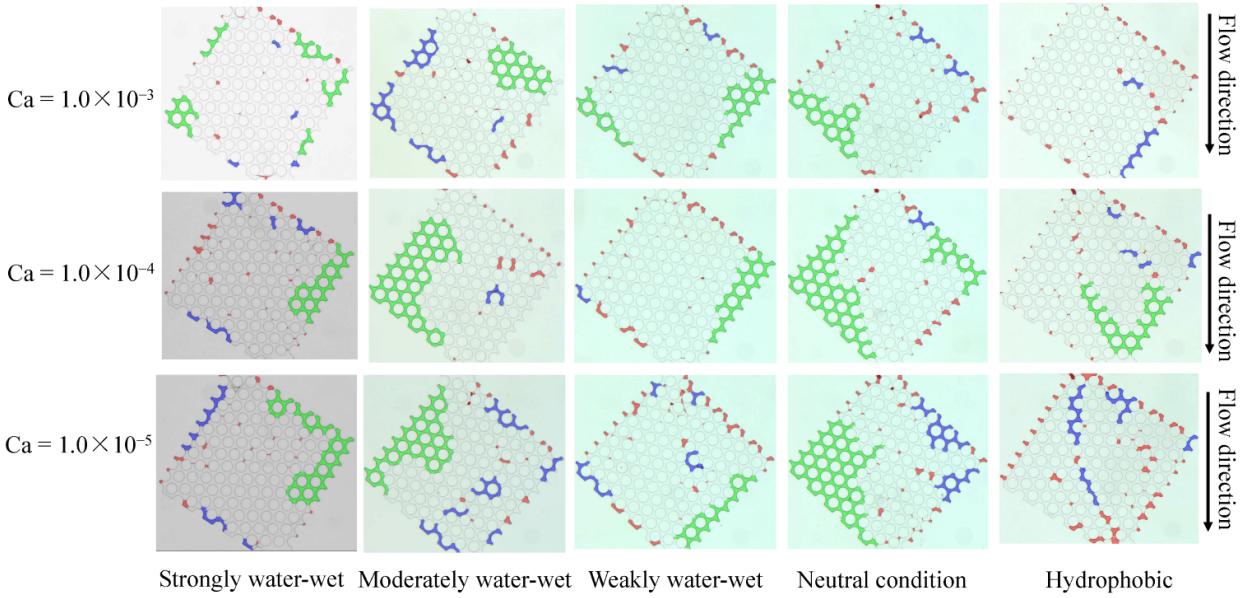

Fig. 7. The classification of different CO_2 distribution patterns after water flooding at different displacement flow rates. Different colors are used to classify CO_2 distribution into three modes: Continuous distribution (green), clustered distribution (blue), and isolated CO_2 bubble distribution (red).

saturation exhibits generally consistent trends across other wettability conditions (Fig. 8(b)). Compared to cluster-like and isolated bubble distributions, a continuous distribution pattern contributes more significantly to the capillary trapping of CO_2. The saturation of continuously distributed CO_2 exhibits two distinct trends with changes in wettability: Initially increasing followed by decreasing, and a decreasing trend (Fig. 8(d)). To clarify the influence of wettability on cluster-like and isolated distributions, images at the minimum displacement flow rate ($Ca = 1.0 \times 10^{-5}$) were selected for analysis. The overall trend for the total saturation of cluster-like and isolated bubble distributions is an increase with increasing contact angle (Fig. 8(d)).

3.3 Mechanism of CO_2 distribution

Wettability also influences the capillary trapping and distribution of CO_2. The visualization experimental results showed that, during the displacement of a non-wetting phase by a wetting phase, variations in the capillary number can induce transitions of the wetting phase flow regime, including viscous fingering to capillary fingering, stable displacement to capillary fingering, and viscous fingering to stable displacement. This study investigates water (wetting phase) displacing CO_2 (non-wetting phase) in microfluidic models with varying wettability. Both numerical simulations and micro-visualization experiments indicate that, under any wettability condition, the residual trapped CO_2 saturation increases with decreasing capillary number. At high capillary numbers, the fluid interface advances uniformly, while at low capillary numbers, the fluid interface advances non-uniformly. As the capillary number decreases, water gradually transitions from a stable displacement mode to a capillary fingering mode, resulting in an increase in the residual trapped CO_2 saturation (Fig. 9(a)).

In our designed displacement experiments, the capillary number is in the order of magnitude of greater than 10^{-7}. Furthermore, the pore walls of the micromodel are relatively smooth, and the viscosity of the invading fluid (water) is also low. The primary trapping mechanism is bypassing trapping caused by the coalescence between extended water fingers, with a secondary mechanism of pore-scale snap-off trapping caused by preceding film flow. Therefore, the saturation of continuously distributed CO_2 is greater than the saturation of cluster-like and isolated bubble distributions, and it is the main contributor to the total residual trapped CO_2 saturation. Cooperative pore filling is an important reason for the occurrence of bypassing. The stronger the wettability of the model, the smaller the contact angle of the invading fluid, which is more conducive to the merging of two adjacent interfaces into a new interface (Fig. 9(b)). This expands the frontal width on the pore network, resulting in more complete waterflooding and lower CO_2 saturation. Therefore, the total residual trapped CO_2 saturation and continuous distribution saturation of the strongly hydrophilic model are greater than those of the hydrophobic model. A smaller contact angle enables invading water to coalesce neighboring menisci into a larger one, thereby broadening the displacement front at the pore-network scale.

Cluster-like and isolated bubble distributions are caused by snap-off induced by preceding film flow. The stronger the hydrophilicity, the stronger the attraction between liquid molecules and the solid. Under wetting conditions, the water phase will rapidly spread and extend on both sides of the tube wall, forming a water film, while the gas occupies the middle position of the tube as a non-wetting phase. As the water phase invades, the water phase saturation within the capillary increases, and the water phase (water film) on both

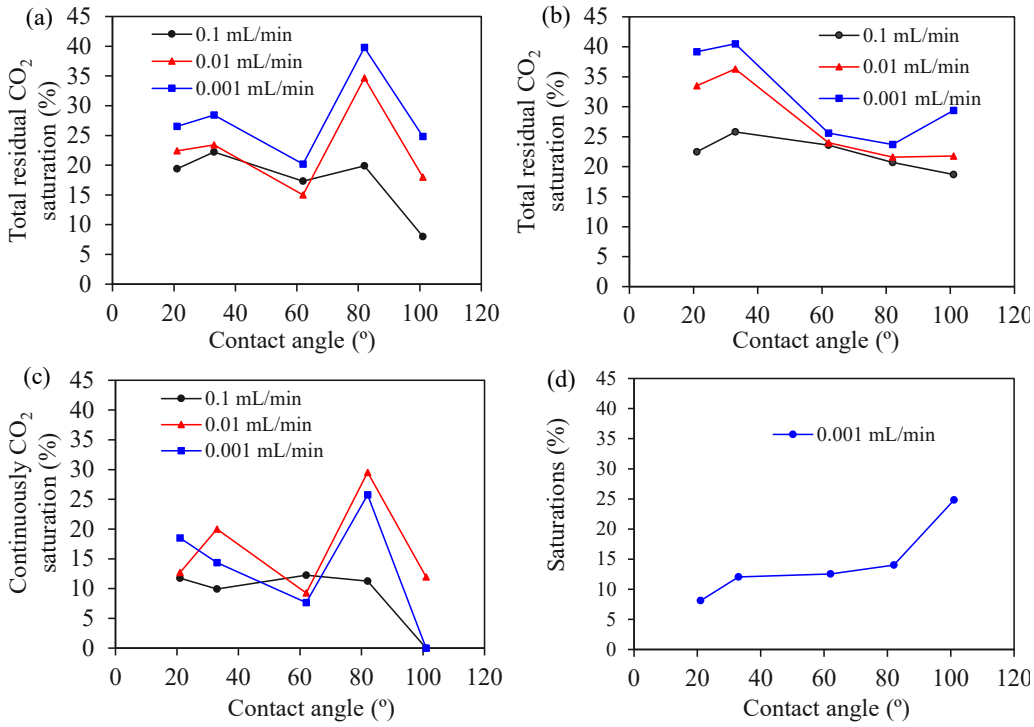

Fig. 8. CO_2 saturation calculation results from models of varying wettability (a)-(b) Experimental and Numerical simulation results of the total residual CO_2 saturation, (c) experimental results of the continuous CO_2 saturation and (d) experimental results of the sum of cluster and isolated CO_2 saturations.

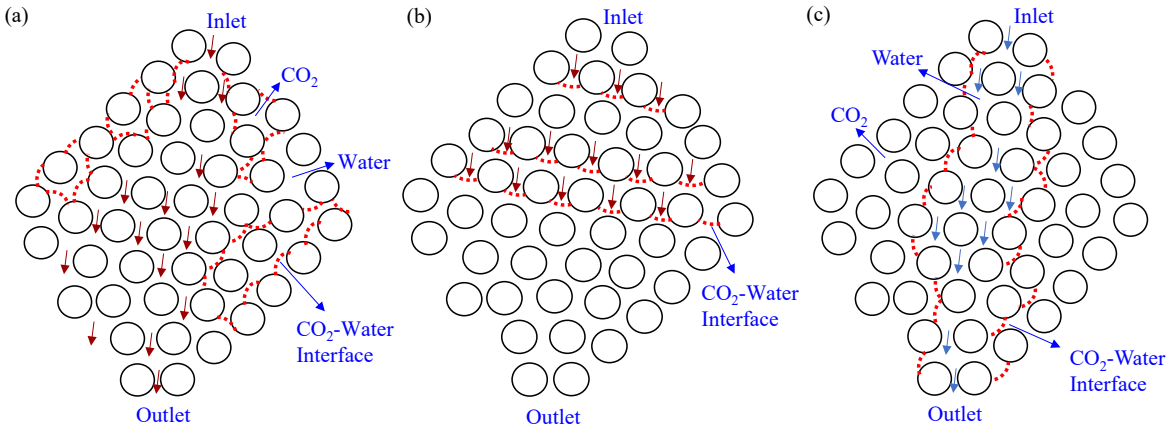

Fig. 9. Diagram of CO_2 distribution mechanism during water reflux process: (a) Non-uniform advancement of CO_2-water interface, (b) uniform advancement of CO_2-water interface and (c) cluster-like and isolated distributed bubbles under the snap-off action.

sides of the tube-wall gradually thickens and compresses the gas in the middle. Because the throat has the smallest size, the water film preferentially coalesces at the throat under the same expansion rate, thereby snapping off the continuous gas phase. In hydrophilic micromodels, water first forms a water film along the fracture walls. As the water film gradually thickens, it gradually spreads and flows along the walls due to wetting. In this process, the gas phase is gradually compressed or displaced, and some throats experience gas snap-off due to the expansion of the water film, generating a discontinuous gas phase. As wettability decreases, the preceding film effect weakens, resulting in the phases not being able to be compressed and displaced, forming more and more cluster-like and isolated distributed bubbles under the snap-off action (Fig. 9(c)).

At high flow rates (high Ca), viscous forces overshadow wettability effects during water-driven CO_2 displacement, reducing its influence on capillary trapping (Fig. 7). The displacement pattern consequently shifts from capillary fingering to stable, viscous-dominated flow in both water-wet and weakly water-wet micromodels. Even in hydrophobic micromodels, increasing displacement flow rates suppress CO_2

trapping. Consequently, the differences in capillary trapping under the three wettability conditions diminish with increasing Ca values. Furthermore, increased flow rates generally promote mobilization of the trapped phase, thus leading to a gradual reduction in the saturation of continuously distributed CO_2 and the number of isolated CO_2 bubbles during water flooding (Fig. 5).

4. Conclusions

This study employed microscopic visualization systems and numerical simulations to visualize and quantify the effects of wettability and capillary number on pore-scale CO_2 distribution. Water flooding experiments in strongly water-wet, moderately water-wet, weakly water-wet, neutral condition, and hydrophobic homogeneous micromodels pre-filled with CO_2, yielded images of the water invasion morphology and trapped CO_2, clearly demonstrating the significant influence of wettability and capillary number on CO_2 distribution. According to experimental and numerical results, the saturation of capillary-trapped CO_2 rises with lower capillary numbers and varies non-monotonically with larger wetting angles in the micromodel. CO_2 exists in three distinct distribution modes: Continuous, cluster-like, and as isolated bubbles. The continuous distribution mode makes the largest contribution to trapping. As contact angle decreases, the cooperative pore filling effect is enhanced, promoting bypassing, which leads to a decrease in the total residual CO_2 saturation and the saturation of continuously distributed CO_2. The variations in cluster-like and isolated bubble CO_2 saturations are due to snap-off induced by preceding film flow. At lower capillary numbers, the combined saturation of clustered and isolated CO_2 bubbles increases with increasing contact angle. In future studies on pore-scale CO_2 distribution during water reflux, factors such as temperature, pressure, and fluid salinity in microfluidic experiments and numerical simulations could be modified for investigation.

Acknowledgements

The authors are grateful for the financial support from the National Nature Science Foundation of China (No. 42372151 and Distinguished Young Scholars (Overseas)), and National Key Research and Development Program of China (No. 2024YFE0107600). They also acknowledge research funding from the Key Research and Development Program of Ordos (No. YF20240035).

Additional information: Author's email

kaiqiang.zhang@pku.edu.cn (K. Zhang)

Conflict of interest

The authors declare no competing interest.

References

Armstrong, R. T., Apostolos, G., Holger, O., et al. Critical capillary number: Desaturation studied with fast X-ray computed microtomography. Geophysical Research Letters, 2014, 41: 55-60.

Ayush, V., Francesco, S. Effect of surface properties on nanoparticle-cell interactions. Small, 2010, 6: 12-21.

Blunt, M. J., Scher, H. Pore-level modeling of wetting. Physical Review E, 1995, 52(6): 6387.

Cai, J., Qin, X., Xia, X., et al. Numerical modeling of multiphase flow in porous media considering micro- and nanoscale effects: A comprehensive review. Gas Science and Engineering, 2024a, 131: 205441.

Cai, J., Zhao, J., Zhong, J., et al. Microfluidic experiments and numerical simulation methods of pore-scale multiphase flow. Capillarity, 2024b, 12(1): 1-5.

Chang, C., Timothy, J. K., Wan, J., et al. Impacts of mixed-wettability on brine drainage and supercritical CO_2 storage efficiency in a 2.5-D heterogeneous micromodel. Water Resources Research, 2020, 55: e2019WR026789.

Chaudhary, K., Cardenas, M. B., Wolfe, W. W., et al. Pore-scale trapping of supercritical CO_2 and the role of grain wettability and shape. Geophysical Research Letters, 2013, 40: 3878-3882.

Chen, K., Zhang, Y., Zhang, J. Pore-scale micromodel experiments for recovery performance evaluation of carbonated water injection for carbon utilization and storage. Chemical Engineering Research and Design, 2025, 221: 472-486.

Drange. H., Alendal, G., Johannessen, O. M. Ocean release of fossil fuel CO_2: A case study. Geophysical Research Letters, 2001, 28: 2637-2640.

Geistlinger, H., Ataei D. I., Mohammadian, S., et al. The impact of pore structure and surface roughness on capillary trapping for 2-D and 3-D porous media. Water Resource Research, 2015, 51: 9094-9111.

Hu, R., Wan, J., Kim, Y. M., et al. Wettability impact on supercritical CO_2 capillary trapping: Pore-scale visualization and quantification. Water Resources Research, 2017, 53: 6377-6394.

Iglauer, S., Fernø, M., Shearing, P., et al. Comparison of residual oil cluster size distribution, morphology and saturation in oil-wet and water-wet sandstone. Journal of Colloid and Interface Science, 2012, 375(1): 187-192.

Lei, W., Gong, W., Wang, M., et al. Wettability effect on displacement in disordered media under preferential flow conditions. Journal of Fluid Mechanics, 2023, 975: A33.

Lei, W., Lu, X., Gong, W., et al. Triggering interfacial instabilities during forced imbibition by adjusting the aspect ratio in depth-variable microfluidic porous media. Proceedings of the National Academy of Sciences of the United States of America, 2024, 120(50): e2310584120.

Li, L., Zhang, D., Su, Y., et al. Microfluidic insights into CO_2 sequestration and enhanced oil recovery in laminated shale reservoirs: Post-fracturing interface dynamics and micro-scale mechanisms. Advances in Geo-Energy Research, 2024, 13(3): 203-217.

Li, S., Liu, H., Wu, R., et al. Prediction of spontaneous imbibition with gravity in porous media micromodels. Journal of Fluid Mechanics, 2022a, 952: A9.

Li, S., Hu, Z., Lu, C., et al. Microscopic visualization of greenhouse-gases induced foamy emulsions in recovering unconventional petroleum fluids with viscosity additives. Chemical Engineering Journal, 2021, 411: 128411.

Li, S., Wang, L., Su, L., et al. Carbon dioxide diffusions in methane-dissolved pore fluids: Implications for geological carbon storage and utilization in tight formations. Chemical Engineering Journal, 2022b, 429: 132147.

Magali, C., Yukie, T. Waterflood oil recovery from mixed-wet limestone: Dependence upon the contact angle. Energy & Fuels, 2017, 31(2): 1529-1535.

Mohsen, S. Y., Arben, J., Shane, P. D., et al. Konicek1Solid with infused reactive liquid (SWIRL): A novel liquid-based separation approach for effective CO_2 capture. Science Advances, 2022, 8: eabm0144.

Ng, K., Payatakes, A. Stochastic simulation of the motion, breakup and stranding of oil ganglia in water-wet granular porous media during immiscible displacement. AIChE Journal, 1980, 26(3): 419-429.

Pak, T., Butler, I. B., Geiger, S., et al. Droplet fragmentation: 3D imaging of a previously unidentified pore scale process during multiphase flow in porous media. Proceedings of the National Academy of Sciences of the United States of America, 2015, 112(7): 19470-19452.

Perrin, J. C., Benson, S. An experimental study on the influence of sub-core scale heterogeneities on CO_2 distribution in reservoir rocks. Transport in Porous Media, 2010, 82(1): 93-109.

Peter, C. Navier-Stokes equations and area of interfaces. Communications in Mathematical Physics, 1990, 129: 241-266.

Plug, W. J., Bruining, J. Capillary pressure for the sand-CO_2-water system under various pressure conditions. Application to CO_2 storage. Advances in Water Resources, 2007, 30(11): 2339-2353.

Rahman, T., Lebedev, M., Barifcani, A., et al. Residual trapping of supercritical CO_2 in oil-wet sandstone. Journal of Colloid and Interface Science, 2016, 469: 63-68.

Sabine, C. L., Tanhua, T. Estimation of anthropogenic CO_2 inventories in the ocean. Annual Review of Marine Science, 2010, 2: 175-198.

Salathiel, R. A. Oil recovery by surface film drainage in mixed-wettability rocks. Journal of Petroleum Technology, 1973, 25(10): 1216-1224.

Shi, J., Xue, Z., Durucan, S. Supercritical CO_2 core flooding and imbibition in Tako sandstone-influence of sub-core scale heterogeneity. International Journal of Greenhouse Gas Control, 2011, 5(1): 75-87.

Suekane, T., Furukawa, N., Tsushima, S., et al. Application of MRI in the measurement of two-phase flow of supercritical CO_2 and water in porous rocks. Journal of Porous Media, 2009, 12(2): 143-154.

Tannaz, P., Luiz, F. L., Tiziana, T., et al. Pore-scale investigation of the use of reactive nanoparticles for in situ remediation of contaminated groundwater source. Proceedings of the National Academy of Sciences of the United States of America, 2020, 117: 13366.

Tokunaga, T. K., Wan, J. Capillary pressure and mineral wettability influences on reservoir CO_2 capacity. Reviews in Mineralogy and Geochemistry, 2013, 77(1): 481-503.

Wang, K., You, Q., Long, Q., et al. Experimental study of the mechanism of nanofluid in enhancing the oil recovery in low permeability reservoirs using microfluidics. Petroleum Science, 2023a, 20: 382-395.

Wang, S., Tokunaga, T. K., Wan, J., et al. Capillary pressure-saturation relations in quartz and carbonate sands: Limitations for correlating capillary and wettability influences on air, oil, and supercritical CO_2 trapping. Water Resource Research, 2016, 52: 6671-6690.

Wang, Z., Li, S., Jin, Z., et al. Oil and gas pathway to net-zero: Review and outlook. Energy Strategy Reviews, 2023b, 45: 101048.

Wardlaw, N., McKellar, M. Oil blob populations and mobilization of trapped oil in unconsolidated packs. The Canadian Journal of Chemical Engineering, 1985, 63(4): 525-532.

Yuan, S., Zhou, F., Ma, M., et al. An experimental study on the imbibition characteristics in heterogeneous porous medium. Physics of Fluids, 2023, 35: 113604.

Zhang, C., Oostrom, M., Wietsma, T. W., et al. Influence of viscous and capillary forces on immiscible fluid displacement: Pore-scale experimental study in a water-wet micromodel demonstrating viscous and capillary fingering. Energy & Fuel, 2011, 25(8): 3493-3505.

Zhang, K., Jia, N., Li, S., et al. Static and dynamic behavior of CO_2 enhanced oil recovery in shale reservoirs: Experimental nanofluidics and theoretical models with dual-scale nanopores. Applied Energy, 2019, 255: 113752.

Zhang, K., Tian, L., Liu, L. R. A new analysis of pressure dependence of the equilibrium interfacial tensions of different light crude oil-CO_2 systems. International Journal of Heat and Mass Transfer, 2018, 121: 503-513.

Zou, S., Zhang, Y., Ma, L. Revealing subsurface dynamics: Imaging techniques for optimizing underground energy storage. Advances in Geo-Energy Research, 2024, 12(1): 1-7.